

M. R. Bown · C. D. Meinhart

AC electroosmotic flow in a DNA concentrator

Received: 17 January 2006 / Accepted: 30 March 2006
© Springer-Verlag 2006

Abstract Experimental velocity measurements are conducted in an AC electrokinetic DNA concentrator. The DNA concentrator is based upon Wong et al. (Transducers 2003, Boston, pp 20–23, 2003a; Anal Chem 76(23):6908–6914, 2004) and consists of two concentric electrodes that generate AC electroosmotic flow to stir the fluid, and dielectrophoretic and electrophoretic force fields that trap DNA near the centre of the inside electrode. A two-colour micro-PIV technique is used to measure the fluid velocity without a priori knowledge of the electric field in the device or the electrical properties of the particles. The device is also simulated computationally. The results indicate that the numerical simulations agree with experimental data in predicting the velocity field structure, except that the velocity scale is an order of magnitude higher for the simulations. Simulation of the dielectrophoretic forces allows the motion of the DNA within the device to be studied. It is suggested that the simulations can be used to study the phenomena occurring in the device, but that experimental data is required to determine the practical conditions under which these phenomena occur.

Keywords Micro-PIV · DNA concentration · AC electroosmosis · Dielectrophoresis · AC electrokinetics

1 Introduction

Electrokinetic phenomena can be used both to drive fluid flow and manipulate particles and molecules. AC and DC electroosmosis, electrothermal effects and electrowetting can be used to create flow, whilst electrophoresis and dielectrophoresis can be used to manipulate particles and molecules (Wong et al. 2003a, 2004).

AC electroosmosis has emerged over the past several years as a method for the driving of fluids in microfluidic devices. The phenomenon occurs at frequencies below the charge relaxation frequency of the electrolyte solution, and can drive fluids with voltages of 5 V or less, compared to the hundreds to thousands of volts often required in DC electroosmosis. In AC electrokinetics, frequencies can be used that are sufficiently high to avoid irreversible electrochemical reactions at the electrode interface, which minimizes electrolysis. This allows the electrodes to be positioned inside the microfluidic device, and therefore, high electric fields can be generated with relatively small voltages.

The motion of particles and fluids subjected to AC electric fields is determined by a combination of AC electrokinetic effects. Electroosmotic or electrothermal forces can induce fluid motion. At low frequencies and low potentials, the electroosmotic forces are dominant (Ramos et al. 1999). A complete computation of an AC electroosmotic flow would require coupled simulations of the electric field, charge density, conductivity and fluid velocity within the electrical double layer, as well as computations of the electric field and fluid velocity in the bulk of the device. An alternative is to use a linear capacitance approximation for the double layer and a fluid slip boundary condition based upon the potential gradient across the electrode surface (González et al. 2000; Green et al. 2002). Particles are not affected by conventional electrophoresis, since the net electric field is zero, but they do experience dielectrophoretic forces. Dielectrophoresis (DEP) arises from a difference in

M. R. Bown (✉)
Department of Chemical and Process Engineering,
University of Sheffield, Newcastle Street, Sheffield S1 3JD, UK
E-mail: markbown@cantab.net
Tel.: +44-114-2227552
Fax: +44-114-2227501

C. D. Meinhart
Department of Mechanical Engineering,
University of California at Santa Barbara, Santa Barbara, CA
93106-5070, USA

electrical permittivity between a particle and the surrounding medium. Under positive DEP the particle is more polarisable than the medium and the DEP force is directed towards regions of high electrical field strength. Conversely, if the particle is less polarisable than the medium, negative DEP occurs and the force is directed down the electric field gradient (Green and Morgan 1997). A review of AC electrokinetic forces and their application to biotechnology can be found in Wong et al. (2003b).

Dielectrophoresis has been demonstrated by concentrating and trapping particles (Cummings et al. 2002) and electrothermal flows have been used to trap sub-micrometre particles in vortices (Müller et al. 1996a). Viruses have also been manipulated using electrokinetic effects (Müller et al. 1996b; Green et al. 1997) and AC electroosmotic stagnation points have been used to trap bacteria (Wu et al. 2005).

DNA sample concentration has been carried out in microdevices using a porous membrane structure (Khandurina et al. 1999), microfluidic filtration (Przekwas et al. 1999) and an affinity microchip (Ito et al. 2004). Dai et al. (2003) reported the concentration of DNA samples based on a balance between electrophoretic and DC electroosmotic velocities, while Han and Craighead (2000) used entropic trapping in a microchannel containing a series of constrictions and wider regions to separate DNA according to its length. The dielectrophoretic trapping of DNA on strips of thin gold films (Asbury and Van Den Engh 1998) and in small quartz constrictions (Chou et al. 2002) has also been demonstrated. Wong et al. (2003a, 2004) developed an AC electroosmotic processor for biomolecules. This AC electroosmotic flow pushes bioparticles towards the centre of a circular electrode, where they are held down by the dielectrophoretic force. The processor has been successfully demonstrated by concentrating samples of double and single stranded DNA molecules.

Lab-on-a-chip DNA sensing typically involves fluorescent labelling of DNA molecules. Individual labelling followed by intensity measurements can determine the length of the molecules (Foquet et al. 2002), whilst sequence specific labelling can be used to detect the presence of a particular genetic sequence on a DNA molecule stretched out in a microchannel (Tegenfeldt et al. 2001). A comprehensive review of the use of micro and nanofluidics in the analysis of DNA is provided by Tegenfeldt et al. (2004).

Micron resolution particle image velocimetry (micro-PIV) is a tool for measuring fluid velocities in microscale geometries with a resolution of a few microns (Santiago et al. 1998; Meinhart et al. 1999). The technique involves obtaining a series of images of a flow seeded with tracer particles. Cross correlation allows the displacement of the particles between images to be determined. In steady flows the averaging of correlation functions from a series of images can significantly improve the quality of the data obtained (Meinhart et al. 2000a). Particle velocity measurements

have been made in AC electroosmotic flows for the purpose of assessing computational techniques (Green et al. 2000, 2002) and in real devices (Wong et al. 2003a, 2004). However, in these measurements no correction is made for the fact that particles in an AC field will experience DEP forces and hence will not follow the fluid motion accurately. In DC electroosmosis the electrophoretic velocity of the particles can be calculated and subtracted from the PIV measurements to obtain the true fluid velocity (Devasenathipathy et al. 2002). However, in AC fields the DEP force depends on the Clausius–Mossotti factor of the particle and the electric field can be more complicated. A solution is to use two-colour micro-PIV (Meinhart et al. 2003; Wang et al. 2005) to measure the fluid velocity uniquely. The technique uses two different sizes of particles coloured with different fluorescent dyes. Since the hydrodynamic drag varies with diameter and the DEP force with particle volume, the fluid velocity can be estimated uniquely from knowledge of the particle velocities and particle diameters, and without any a priori knowledge of the electric field or the electrical properties of the particles.

Wong et al. (2003a, 2004) developed an AC electroosmotic processor for biomolecules. The processor uses AC electroosmotic flow to push particles towards the centre of a circular electrode, where they are held down by the dielectrophoretic force. When manipulating short, single strands of DNA, the DEP force is insufficient to hold the molecules down over the electrode and an electrophoretic force must be introduced. They present the physical principles on which the bioprocessor is based, along with a numerical simulation and experimental demonstration of its operation.

Here, we extend the work of Wong et al. (2003a, 2004) by examining in detail the fluid motion in the AC electroosmotic bioprocessor. The device is studied using the two-colour micro-PIV technique (Wang et al. 2005) to measure accurately the fluid velocity field. The physics of the flow are modelled using a thin double layer approximation and slip boundary condition. A direct comparison of the results allows the accuracy of the simulation strategy and the errors associated with using PIV measurements of only one particle size to be discussed.

2 AC electroosmosis and dielectrophoresis

AC electroosmosis is a flow phenomenon that occurs below the charge relaxation frequency of a fluid (Ramos et al. 1998). A charged double layer forms on the surface of an electrode. This double layer interacts with the small transverse component of the electric field to produce a fluid motion across the electrode surface. Because the sign of the electric field and the charge density change in phase with one another, the fluid motion is always in the same direction (Figs. 1, 2).

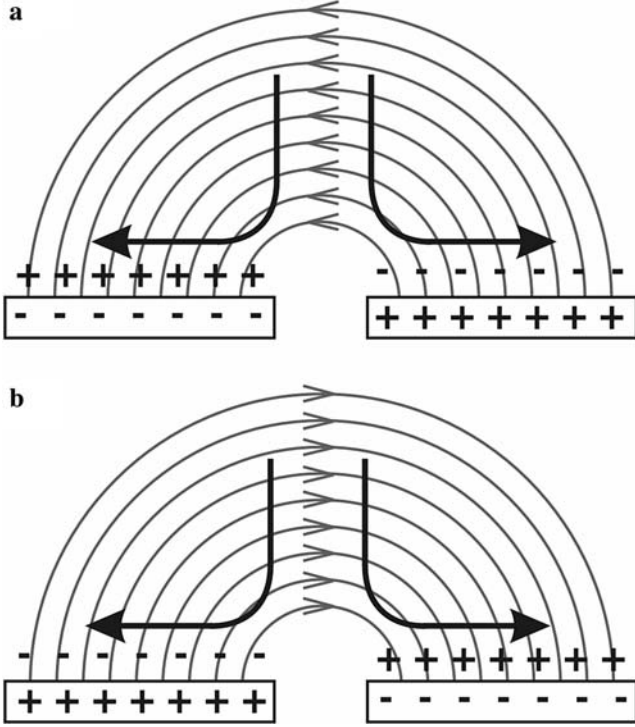


Fig. 1 Interaction of the electric double layer and transverse component of the electric field during AC electroosmotic flow. As the sign of the field switches (a \rightarrow b), the sign of the double layer charge also switches, resulting in a uniform flow direction

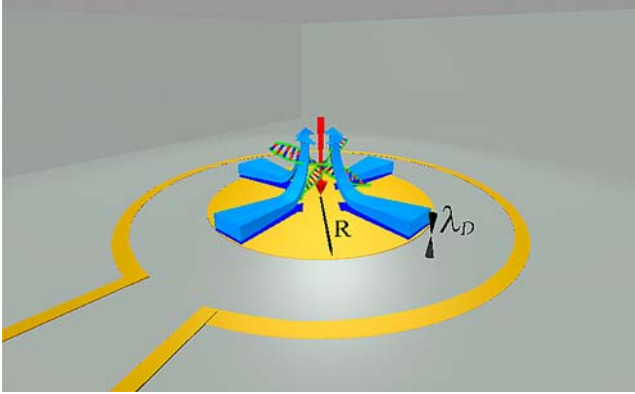


Fig. 2 Electrokinetic bioprocessor. The bulk fluid flow (light blue) is driven by the movement of the double layer (dark blue) towards the centre of the electrode. DNA molecules are carried to the centre of the electrode by the fluid where they are trapped by the vertical component of the DEP force (red arrow)

At very low frequencies all of the potential is dropped across the double layer and the transverse component of the electric field is thus too small to generate flow. At high frequencies, approaching the charge relaxation frequency, the double layer has insufficient time to form and thus there is no charged fluid to interact with the electric field, also resulting in zero flow. AC electroosmotic flow is observed between these two extremities (Ramos et al. 1999). The governing equations of

electroosmotic flow and a possible simulation strategy is proposed by González et al. (2000). When applied in cylindrical polar coordinates to the rotationally symmetric geometry of the bioprocessor, this approach leads to two equations for the electric field and charge density,

$$\frac{\partial^2 \tilde{\phi}'}{\partial z'^2} + \frac{\delta^2}{r'} \frac{\partial}{\partial r'} r' \frac{\partial \tilde{\phi}'}{\partial r'} = -\tilde{\rho}'_f, \quad (1)$$

$$0 = -\tilde{\rho}'_f(1 + i\omega) + \frac{\partial^2 \tilde{\rho}'_f}{\partial z'^2} + \frac{\delta^2}{r'} \frac{\partial}{\partial r'} r' \frac{\partial \tilde{\rho}'_f}{\partial r'}. \quad (2)$$

$\tilde{\phi}'$ is the normalised electric field written in phasor form, $\phi'(t) = \Re\{\tilde{\phi}'e^{i\omega t}\}$ and $\partial\tilde{\phi}'/\partial t = i\omega\tilde{\phi}'$, $\tilde{\rho}'_f$ is the normalised charge density, also written as a phasor and ω is the frequency, normalised by the charge relaxation time, $\tau = \sigma/\varepsilon$. The length scales in the r and z directions are R and λ_D , respectively. The ratio of the length scales is given by $\delta = \lambda_D/R$. The normalisation of the variables is given by

$$\phi = \frac{D}{\mu} \phi', \quad \rho_f = \frac{\sigma}{\mu} \rho'_f, \quad t = \frac{\varepsilon}{\sigma} t', \quad \omega = \frac{\sigma}{\varepsilon} \omega', \quad (3)$$

$$z = \lambda_D z', \quad r = R r', \quad \lambda_D = \sqrt{\frac{\varepsilon D}{\sigma}}, \quad \delta = \frac{\lambda_D}{R}.$$

σ is the conductivity, μ the ion mobility, D the diffusivity and ε the electrical permittivity of the fluid. The approach has assumed a symmetric electrolyte and constant conductivity within the double layer. The convective component in the ion fluxes is also assumed to be small, and the electric field can thus be solved independently of the flow field. González et al. (2000) introduce the non-dimensional frequency, $\Omega = \omega R \sqrt{1 + i\omega}/\lambda_D$, and an asymptotic matching boundary condition,

$$\partial\tilde{\phi}'/\partial z = i\Omega(\tilde{\phi}' - V_j), \quad (4)$$

where V_j is the potential applied to electrode j . This allows the potential field to be solved in the bulk fluid, without the need to simulate the double layer. The fluid flow is solved for the bulk only, using a slip boundary condition at the electrode (Green et al. 2002)

$$u_{\text{slip}} = -\frac{\varepsilon}{2\eta} \Lambda \Re\left\{\Delta\tilde{\phi}'_{\text{DL}} \frac{\partial\tilde{\phi}^*}{\partial r}\right\}. \quad (5)$$

Here, Λ is a factor to account for the Stern layer and is taken as 0.25 in the current work, following Green et al. (2002). The electric potential drop across the double layer is given by $\Delta\tilde{\phi}'_{\text{DL}} = \tilde{\phi}' - V_j$.

The outer problem (i.e. outside the double layer) is simulated using the finite element software *Femlab V3.1* (Comsol, Stockholm, Sweden) by first solving Laplace's equation for electric potential,

$$\nabla^2 \phi = 0 \quad (6)$$

and then solving the incompressible Stokes equations

and mass continuity for fluid motion

$$\begin{aligned}\nabla p + \mu \nabla^2 \vec{u} &= 0, \\ \nabla \cdot \vec{u} &= 0,\end{aligned}\quad (7)$$

where p is pressure, and μ is dynamic viscosity.

Figure 3 shows the boundary conditions for the outer problem of the DEP concentrator. The problem is axisymmetric around the $r = 0$ axis. The electrode is $300 \mu\text{m}$ in diameter and the working fluid is KCl solution, with a conductivity of $\sigma = 55 \mu\text{S/cm}$. For the electric field, the matching boundary condition, Eq. 4, is applied to the electrode surfaces, electrical insulation is applied to rest of the boundaries. For the Navier–Stokes simulation, the slip boundary condition, Eq. 5, is applied to the electrode surfaces, and no slip to the remaining surfaces. The computation was carried assuming an applied electrode potential of $4 V_{p-p}$ and frequencies ranging from $f = 100 \text{ Hz}$ to 1.6 MHz . The problem is solved using the *Femlab V3.1* parametric solver on a mesh of 6,500 elements, with a higher density of elements near the tip of the electrode.

Figure 4 shows a computation of the potential field and the velocity profile. The simulation was carried out with an applied voltage of 4 V at a frequency of 100 Hz . The maximum velocity is around $6 \mu\text{m/s}$. At higher frequencies the velocity magnitude peaks and the region of high velocity is confined more closely to the electrode tip.

Particles in the bio-processor move under the influence of the fluid and the dielectrophoretic force exerted on them by the electric field. DEP occurs when the polarisability of a particle differs from that of the surrounding fluid. If the particle is more polarisable it will move to regions of high electric field and vice versa. The former is known as positive DEP and the latter as negative DEP (Green and Morgan 1997). The time averaged DEP force is

$$F_{\text{DEP}} = 2\pi a^3 \varepsilon \Re\{K(\omega)\} |\nabla|E_0|^2, \quad (8)$$

where a is the particle radius and $\Re\{K(\omega)\}$ the real part of the Clausius–Mossotti factor,

$$\begin{aligned}u &= -\frac{\varepsilon}{2\eta} \Lambda \operatorname{Re} \left[\Delta \tilde{\phi}_{\text{DL}} \frac{\partial \tilde{\phi}^*}{\partial r} \right] & u &= -\frac{\varepsilon}{2\eta} \Lambda \operatorname{Re} \left[\Delta \tilde{\phi}_{\text{DL}} \frac{\partial \tilde{\phi}^*}{\partial r} \right] \\ \frac{\partial \tilde{\phi}}{\partial z} &= i\Omega \left(\tilde{\phi} - V_0/2 \right) & \frac{\partial \tilde{\phi}}{\partial z} &= i\Omega \left(\tilde{\phi} + V_0/2 \right)\end{aligned}$$

Fig. 3 Boundary conditions for the numerical computations of the potential and velocity fields

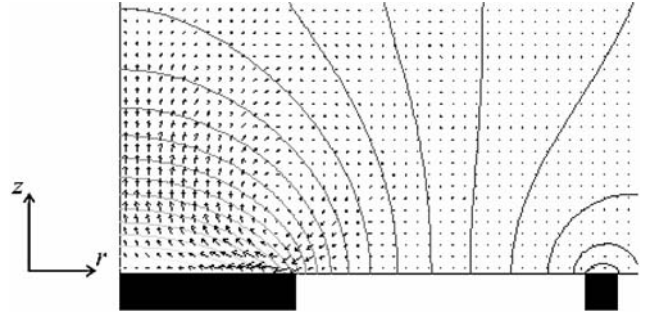


Fig. 4 Computational results for lines of constant electric potential and velocity vectors depicting the flow fields in the AC electrokinetic concentrator. The simulation was carried out with an applied voltage of $4 V_{p-p}$ at a frequency of 100 Hz . The maximum velocity is around $6 \mu\text{m/s}$. At higher frequencies the value of the maximum velocity peaks (see Fig. 10) and the velocity decreases more rapidly across the electrode

$$K(\omega) = \frac{\tilde{\varepsilon}_p - \tilde{\varepsilon}_m}{\tilde{\varepsilon}_p + 2\tilde{\varepsilon}_m}, \quad (9)$$

p denotes the particle and m denotes the medium. The complex permittivity is defined as $\tilde{\varepsilon} \equiv \varepsilon - i\sigma/\omega$. For a sphere, $\Re\{K(\omega)\}$ varies between -0.5 and 1 and determines whether positive or negative DEP occurs (Ramos et al. 1998). The switch between positive and negative DEP with frequency has been demonstrated experimentally (Green and Morgan 1997). In the bio-processor, the fluid drags the particles to the centre of the electrode, where they are then trapped by the positive DEP force. The simulation strategy of González et al. (2000) is extended here to model the DEP forces within the bioprocessor. This requires information on the Clausius–Mossotti factor and shape of the DNA. The conductivity of λ -phage DNA in buffer is measured by Tran et al. (2000) as 2.4 S/cm and the dielectric constant is taken as 4.0 (van der Maarel 1999). Crucially, these values lead to the real part of the Clausius–Mossotti factor, the value needed in Eq. 8, being within 0.01% of 1.0 for the whole range of frequencies studied here and insensitive to small changes in the individual values. This is entirely consistent with experimental observations showing that DNA is expected to undergo positive DEP (Asbury and Van Den Engh 1998; Zheng et al. 2004). The native state of λ -phage is loose spheres of approximately $2\text{--}4 \mu\text{m}$ in diameter (Zheng et al. 2004), a value of $4 \mu\text{m}$ is used here. By equating Eq. 8 and the drag force, $F_{\text{D}} = 6\pi\eta a(u - u_{\text{DNA}})$, the motion of the DNA can be deduced. Figure 5 shows diagrams of the DNA motion at three different frequencies. At low frequency the drag force dominates and the DNA merely circulates within the device. At high frequency the DEP force dominates and the DNA will be attracted to the entire electrode. At intermediate frequencies, the drag force will draw the DNA into the centre of the electrode and the DEP force will keep it there. This represents the optimum concen-

Fig. 5 Computational simulation of the DNA motion within the bioprocessor at 800 Hz (a), 51 kHz (b) and 205 kHz (c). At low frequencies the drag force dominates and the DNA circulates, whilst at high frequencies the DEP force draws the DNA to all points on the electrode. At intermediate frequencies the drag force pulls the DNA to the centre of the electrode and the DEP force holds it down. This is the regime in which the device should operate. Note that, for clarity, the arrows indicate the direction of the DNA motion only

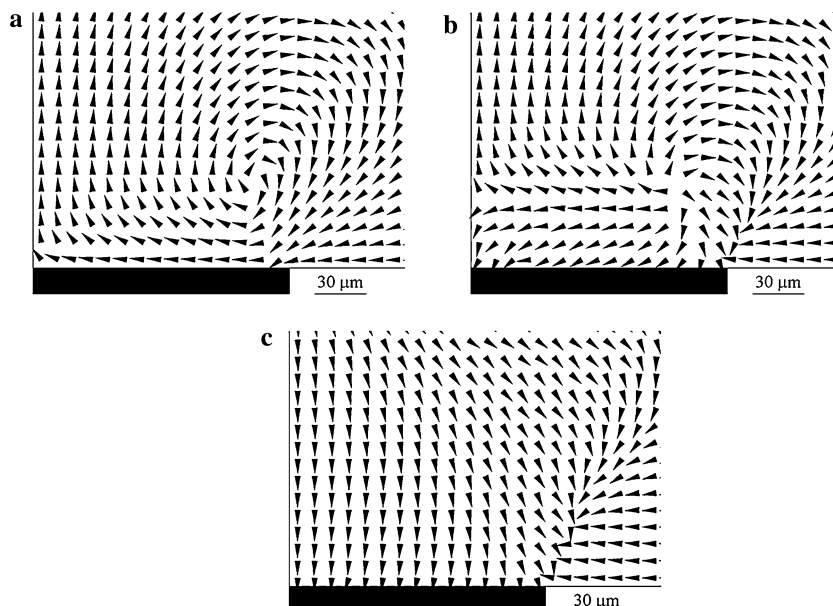
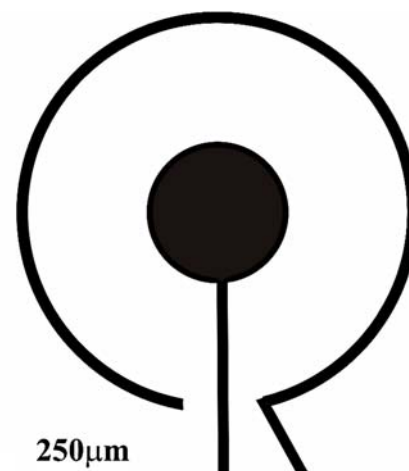
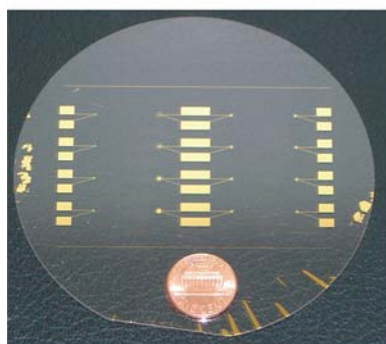


Fig. 6 Design of the DEP concentrator. On the left is a picture of a device with 16 electrodes of varying geometries, the coin is a US cent. The particular electrode geometry used in this work is shown in the diagram on the right



tration strategy and is the regime in which the device should operate.

3 Experimental details

The microfluidic concentrator consists of an inner circular electrode with a second ring electrode around it, based on the design of Wong et al. (2003a, 2004) (Fig. 6). The centre electrode is 300 μm in diameter and the gap between the electrodes is 250 μm . The outer electrode is 25 μm wide and is open on one side to allow electrical connections to be made to the centre electrode. Figure 6 shows a picture of the finished wafer, and a schematic of the electrode configuration.

The device was fabricated on a glass wafer. Electrodes were formed from a 500 \AA titanium layer and a 2,000 \AA gold layer. A transparency mask of the

electrode pattern was printed and exposed onto a layer of photoresist on the glass wafer. The photoresist was then developed and etched away in the region where the electrodes will be located. The wafer was then coated with the titanium and gold and the remaining photoresist etched away. This process was used to deposit the electrode pattern onto the glass wafer. A flow cell was formed using microscope cover slips 170 μm thick as spacers, with another microscope cover slip on top to provide high quality optical access and to reduce evaporation.

The working fluid was an electrolyte solution of water and KCl with an electrical conductivity of 55 $\mu\text{S}/\text{cm}$. A voltage of 4 $V_{\text{p-p}}$ and frequency $f = 10$ Hz was applied to the electrodes. For the λ -phage DNA concentration experiments a 3.3 $\text{ng}/\mu\text{l}$ solution of λ -phage DNA (48.5 kbp, Invitrogen 25250-010) labelled with 1 μM YOYO-1 fluorescent dye (Molecular Probes, Y3601)

was made using the same fluid. A voltage of $4 V_{p-p}$ and frequency $f=1$ kHz, with no DC offset, was applied for 100 s. For the single stranded DNA concentration a 3.3 ng/ μ l solution of a fluorescein labelled 24 base pair M13/pUC sequencing primer was prepared. Concentration of the short DNA only occurred when a DC offset of 0.5 V was superimposed upon the AC field.

In general, tracer particles in the device will move under the influence of the fluid and the DEP force exerted on them by the electric field. In order to obtain the fluid velocity, these forces must be calculated. Calculation of the DEP force requires a numerical simulation of the electric field in the device and knowledge of the Clausius–Mossotti factor of the particles (see Eq. 8).

An alternative is to use the two-colour micro-PIV method introduced by Wang et al. (2005) to measure the fluid flow directly. The fluid is seeded with two sets of particles with the same material properties, but different diameters and dyes. In the current experiment, the flow-tracing particles were 0.50 and 0.86 μ m diameter polystyrene particles, emitting green and red light, respectively (*G500 and R900: Stokes' shift* 40 and 70 nm, Duke Scientific, Palo Alto, CA USA). The particle concentration was 0.005 wt% for both the 0.50 and 0.86 μ m diameter particles. Fluorescent filter cubes (exciters E565LP and HQ450/50M, emitters D535/45M and HQ525/50X Chroma Technology Corp, VT, USA, Dichroic cut-offs 565 and 508 nm, Edmund Optics, York, UK) were selected so that only one colour (i.e. one size) of particle was imaged at any one time, following Wang et al. (2005). A sequence of particle images was recorded of the 0.50 μ m diameter particles moving in the fluid. The filter was then switched, and a second set of images was recorded of the 0.86 μ m diameter particles.

Each sequence of particle-image fields was analyzed separately in order to obtain the particle velocities. If the velocity field of each particle is known, then the velocity of the fluid, u_f , can be estimated by (Wang et al. 2005)

$$u_f = \frac{d^2_{p2} u_{p1} - d^2_{p1} u_{p2}}{d^2_{p2} - d^2_{p1}}, \quad (10)$$

where d are the physical particle diameters, and u are the velocities of the particles. The subscripts $p1$ and $p2$ denote particles of size 1 and size 2, respectively.

Equation 10 is derived by balancing the hydrodynamic drag and the DEP force of the particle, and assuming that the Clausius–Mossotti factor is the same for each size of particle (Wang et al. 2005). The trajectories of the particles are three-dimensional. However, providing that the particles do not become defocused between the two PIV images, the radial component of the velocity can still be measured with the two-dimensional micro-PIV technique. Since the radial and axial components of the DEP force are independent, the combination of the velocity fields using Eq. 10 in two-dimensions is also reasonable. The micro-PIV

measurement depth, over which particles can be detected, for the lens used in this work is 27.4 μ m (Meinhart et al. 2000b) and particles do not become defocused between the two images. The measured PIV velocity will be an average of the radial velocity component across the measurement depth, weighted toward the focal plane (Olsen and Adrian 2000). The error associated with assigning this weighted average to the focal plane is small compared to the experimental uncertainties (Bown et al. 2005).

4 Results

Figure 7 shows the concentration of 48.5 kbp λ -phage DNA. A $4 V_{p-p}$ electric potential is applied at a frequency of 1 kHz, with no DC bias. After 100s the DNA can be clearly seen to have concentrated in the centre of the electrode. The frequency of 1 kHz increases the ratio of the DEP force to the fluid drag force on the DNA, enhancing the trapping effect. The fluorescence intensity has increased by a factor of 6.5 in the centre of the device. This represents an average of the DNA concentration across the depth of the flow cell and does not reflect the fact that the DNA is also being concentrated in the out-of-plane direction. Therefore, 6.5 is a lower bound on the concentration factor, and the true value will be significantly greater than this. Figure 8 shows a similar concentration experiment using the fluorescein labelled 24 base pair M13/pUC sequencing primer. Because the molecule is much smaller than the λ -phage DNA, the dielectrophoretic force alone is not sufficient to hold the single stranded DNA in place above the electrode. Therefore, a DC offset of ± 0.5 V is superimposed on the AC field. This allows the DNA to be concentrated over first the inner and then the outer electrode. The fluorescence intensity increases by a

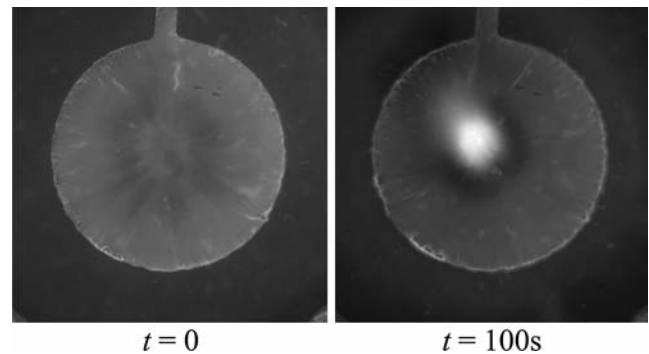


Fig. 7 λ -phage DNA (48.5 kbp, Invitrogen 25250-010) labelled with 1 μ M YOYO-1 fluorescent dye (Molecular Probes, Y3601) being concentrated in the bio-processor. The applied voltage is 4 V peak-to-peak at 1 kHz, with no DC offset. The fluorescence intensity has increased by a factor of 6.5 in the centre of the electrode. Since this represents a depth average, and the DNA is principally close to the electrode, the actual concentration factor will be significantly greater than this

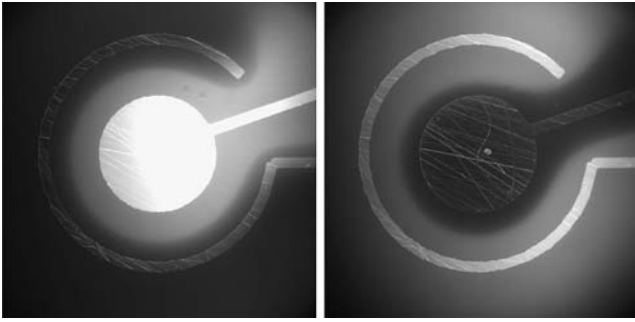


Fig. 8 24 base pair, single stranded, fluorescein labelled M13/pUC sequencing primer concentrating over first the inner and then the outer electrode when a DC offset of ± 0.5 V is applied to the AC voltage. The electrophoretic force due to the DC offset complements the dielectrophoretic force, which alone is too weak to hold the small molecules in position. The fluorescence increases by a factor of 8. Again, this is a depth average and the actual concentration factor will be significantly greater

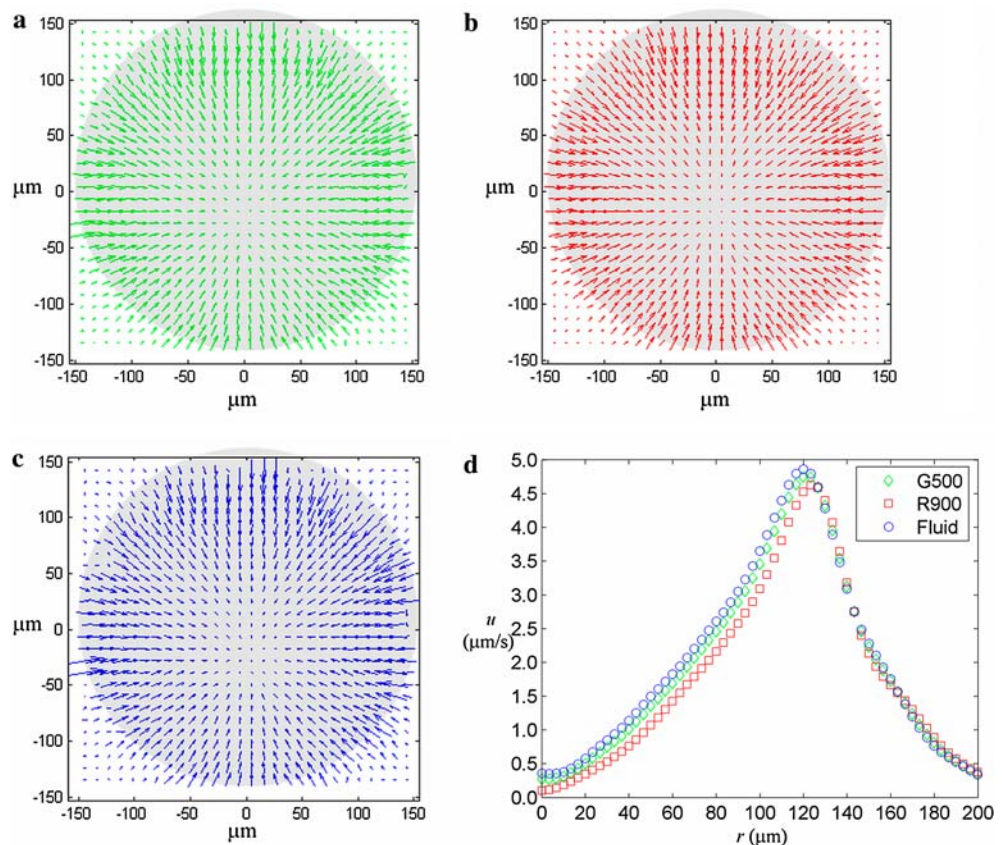
factor of 8. As with the λ -phage DNA, this represents a depth average and thus the actual concentration factor will be greater. It is also noticeable that the DNA concentrates over the entire electrode, not in the centre as was the case for the λ -phage DNA. This suggests that the concentration effect is purely electrophoretic and that the device is not operating in the manner intended (see Fig. 2). Thus, if short DNA is to be concentrated,

the AC field with its corresponding flow patterns and DEP forces becomes unnecessary, and a device specifically designed to carry out an electrophoretic concentration is likely to be of greater use. The velocity measurements will therefore concentrate on the case of large DNA concentration, using the DEP force and no DC offset.

Figure 9 shows the two particle velocity fields and the resulting fluid velocity field in the DEP concentrator operating at 4 V peak-to-peak with a frequency $f=10$ Hz. The flow moves radially into the electrode centre, as predicted from the numerical simulation results, shown in Fig. 4. Figure 8d shows the radial components of velocity as a function of radial position. The radial profiles are obtained by resampling the micro-PIV data based on radial position from the square grid using a Gaussian weighting function with an e^{-1} width of $21 \mu\text{m}$. Even though the velocity-vector plots for both size particles look similar, the particle velocity can be as much as 10% lower than the fluid velocity (see Fig. 9d). This underscores the importance of using two different size particles (Wang et al. 2005).

Figure 10 compares the maximum radial fluid velocity as a function of frequency obtained from the experimental data, with the same information obtained from the numerical simulations. The shape of the two sets of data is similar, but the magnitude of the maximum velocity and the frequency at which it occurs are two

Fig. 9 Velocity vectors and radial velocity profiles for the two particle sizes ($0.50 \mu\text{m}$ green and $0.86 \mu\text{m}$ red) and the fluid velocity field estimated from the combination of the two (blue), measured just above the centre electrode. The shape of the electrode is shown in grey in a-c. The driving voltage is 4 V peak-to-peak with a frequency $f=10$ Hz: **a** velocity-vector field of the $0.50 \mu\text{m}$ diameter green particles, **b** velocity-vector field of the $0.86 \mu\text{m}$ diameter red particles, **c** estimated fluid velocity-vector field, **d** radial velocity profile of the of the particles and fluid



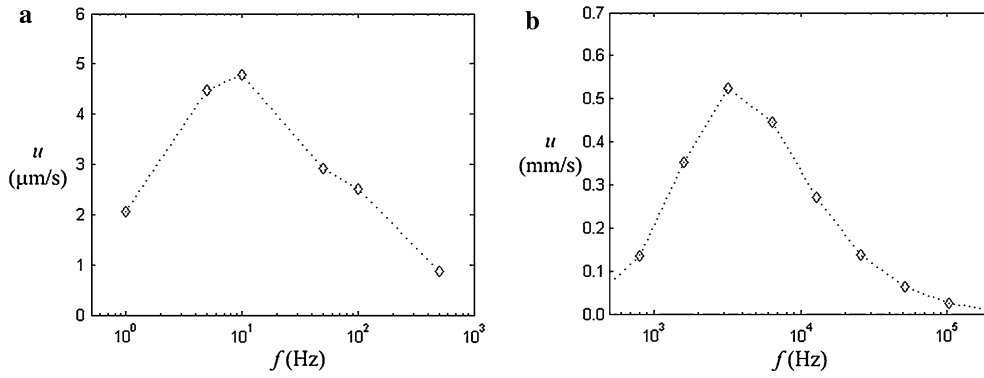


Fig. 10 Maximum radial velocity as a function of frequency in the electrokinetic concentrator: **a** experimental micro-PIV results, **b** numerical simulations. The maximum velocities and peak frequencies from the numerical simulations results are two orders of

magnitude greater than those obtained by experiment. The maximum velocity is $u_{\max} = 5 \mu\text{m/s}$ at a frequency of $f = 10 \text{ Hz}$, and $u_{\max} = 500 \mu\text{m/s}$ at $f = 2,000 \text{ Hz}$, for the experiments and numerical simulations, respectively

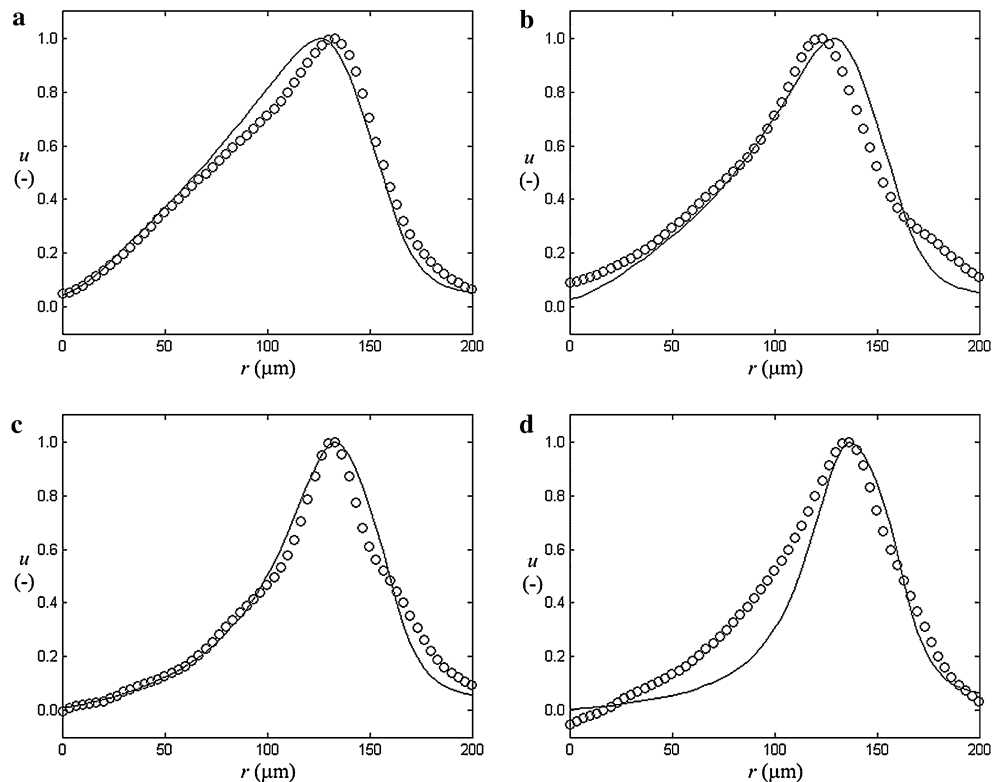
orders of magnitude larger for the computational data. The maximum velocity is $u_{\max} = 5 \mu\text{m/s}$ at a frequency of $f = 10 \text{ Hz}$, and $u_{\max} = 500 \mu\text{m/s}$ at $f = 2,000 \text{ Hz}$, for the experiments and numerical simulations, respectively. The shapes of the velocity profiles obtained are similar between the numerical simulations and experiments.

The results shown in Fig. 10 are similar in shape. Therefore, the experimental and computational velocity profiles were normalized by the maximum velocity. The frequency was scaled to obtain comparable velocity curves (data not shown). This allowed us to compare directly frequencies that were effectively similar for the

computational and experimental results shown in Fig. 10. We chose four representative frequencies from the experimental data, $f = 5, 10, 50, 100 \text{ Hz}$. Four representative frequencies from the numerical simulations that compare to the experiments were found to be $f = 1.6, 3.2, 56.4, 12.8 \text{ kHz}$.

Figure 11 shows the normalized radial velocity profiles of the experimental micro-PIV data and the numerical simulations, at the comparable frequency pairs listed above. The shapes of the velocity profiles and the variation of velocity with frequency are similar in both the computational and experimental results. The

Fig. 11 Computational (*line*) and experimental (*Open circles*) velocity profiles at approximately equivalent frequencies as determined from Fig. 10: **a** experiment $f = 5 \text{ Hz}$, computation $f = 1.6 \text{ kHz}$, **b** experiment $f = 10 \text{ Hz}$, computation $f = 3.2 \text{ kHz}$, **c** experiment $f = 50 \text{ Hz}$, computation $f = 6.4 \text{ kHz}$, **d** experiment $f = 100 \text{ Hz}$, computation $f = 12.8 \text{ kHz}$



shape of the velocity profiles are also in agreement with previous observations of particle motion across electrodes (Green et al. 2000). However, the frequencies at which flow occurs and the magnitude of the velocities obtained are two orders of magnitude lower in the experimental data than in the computations. A similar frequency effect may be observed in previous work using this method of simulation (Green et al. 2002).

5 Discussion

Figure 9 shows that the particle velocity can differ by as much as 10% from the estimated fluid velocity near the centre electrode, where DEP forces are significant. The particles in this region typically move more slowly than the fluid. This is because the electric field gradient (i.e. DEP force) is strongest at the edge of the electrode. The DEP force that attracts the particles to the centre electrode also retards the particle velocity towards the centre of the electrode. The $0.86\ \mu\text{m}$ diameter particles are larger than the $0.50\ \mu\text{m}$ diameter particles, and thus experience a greater DEP force relative to the Stokes drag force. Hence, the velocity of the $0.86\ \mu\text{m}$ diameter particles is lower than that of the $0.50\ \mu\text{m}$ diameter particles. Subsequently, it is important to use the two particle technique to determine velocity fields accurately in many AC electrokinetic flows.

The error due to DEP forces can be reduced by using smaller particles, say 200 nm diameter particles, such as Wong et al. (2003a, 2004). However, smaller particles can be undesirable for a number of reasons. Because of their small size, smaller particles emit less light, and can be more difficult to image, especially with low numerical aperture lenses. In addition, the diffusion due to Brownian motion scales as $\sim 1/d_p$. By using larger particles, the stochastic errors associated with Brownian motion can be traded for deterministic errors due to DEP forces. However, the DEP forces can be accounted for by using the two-size micro-PIV technique.

The maximum radial velocity was measured to approximately $5\ \mu\text{m/s}$ for an applied voltage of $4\ V_{p-p}$, a frequency of $f=10\ \text{Hz}$, and for an electrical conductivity of $\sigma=55\ \mu\text{S/cm}$. The magnitude of this velocity is in reasonable agreement with the data reported by Wong et al. (2003a, 2004). The characteristic velocities predicted by the numerical computations are approximately $500\ \mu\text{m/s}$, using the model introduced by González et al. (2000). This is of two orders of magnitude different in scale. In addition, the frequencies at which the peak velocities occur are also several orders of magnitude higher in the numerical computations than observed in the experiments. This is consistent with previous observations (see Wong et al. 2003a, 2004).

Even though the velocity and frequency scales between the experimental data and the numerical computations are different, the relative shapes of the radial velocity profiles are similar. Figure 11 compares

the radial velocity profiles of the experimental data to the computational results, for approximately equivalent frequencies obtained from Fig. 10. The shape of the profiles look quite similar for the frequencies examined. The velocity profiles peak at approximately $r\sim 140\ \mu\text{m}$, and are skewed towards the electrode centre.

The discrepancy between the theoretical predictions of AC electroosmosis and the experimental micro-PIV results, suggests the need for more accurate handling of the electric double layer. The modelling of AC electroosmosis as a slip boundary condition based on the tangential component of the potential gradient across the electrode surface (see Eq. 5) is a valid approach, but the method for determining the potential drop across the electric double layer, $\Delta\phi_{DL}$, may not be accurate. When introducing the linear approximation used in this work, González et al. (2000) mention that it is only valid for potential drops across the double layer smaller than 25 mV but that insights into the phenomena occurring can still be obtained with the linear model outside of this regime. The non-dimensional results in Green et al. (2002) show the same order of magnitude discrepancy between the computational and experimental results that is found in this work. The computational solutions here show that, in the regime in which AC electroosmosis occurs, the potential drop across the double layer is much greater than the 25 mV limit. It is suggested that, whilst computational studies can model the phenomena that are occurring in the device and be used to optimise its performance, experimental data is needed to determine the practical conditions under which these phenomena occur. Thus Fig. 10 is important, as it allows the parameters required to produce an effect in the computational work to be related to the conditions in the real device at which that effect may be expected to occur. In Fig. 5, the optimum operating conditions for the device were shown to be around 50 kHz in the computations. Using Fig. 10, this corresponds to the frequency region around 1 kHz, which is the frequency at which the λ -phage DNA concentration occurred.

The device has been demonstrated concentrating both λ -phage (48.5 kbp) and single stranded DNA (Figs. 7, 8), although the latter is thought to be concentrated due to electrophoresis. The concentration factor can be estimated from fluorescence intensity measurements. However, this represents a depth average and thus will not take into account any concentration effect in the out-of-plane dimension. For example, if the depth of the device is $100\ \mu\text{m}$ and the DNA is concentrated into the $10\ \mu\text{m}$ above the electrode, the true concentration factor would be approximately 10 times that estimated from the fluorescence intensity measurements. The values obtained do provide a lower bound on the concentration factor, this is found to be 6.5 for the λ -phage DNA and 8 for the single stranded (24 bp) DNA.

6 Conclusions

An AC electrokinetic concentrator (introduced by Wong et al. 2003a, 2004) has been studied using the two-colour micro-PIV technique introduced by Wang et al. (2005). The fluid velocity can be deduced from the velocity fields of two different sized flow-tracing particles, without a priori knowledge of the electric field or the electrical properties of the particles. The results show that the particle velocities differ by as much as 10% from the fluid velocity, for 0.50 and 0.86 μm diameter polystyrene particles. This underscores the importance of using two different size particles for accurate velocity measurements, where DEP forces are significant. The working fluid was a $\sigma = 55 \mu\text{S}/\text{cm}$ electrolyte solution. When an AC voltage of $4 V_{\text{p-p}}$ at a frequency of $f = 10 \text{ Hz}$ was applied to the device, the characteristic AC electroosmotic velocity was approximately $5 \mu\text{m}/\text{s}$. The maximum velocity occurs near the electrode edges and decreases towards zero at the electrode centre. The device has also been demonstrated concentrating λ -phage DNA molecules and 24 base pair, single stranded DNA. Concentration factors of at least 6.5 and 8 are found for the two cases respectively. Since these values result from a depth-averaged fluorescence measurement, the true concentration factors will be significantly greater.

The electric field and velocity field in the outer region of the flow was simulated using the electric double layer matching condition suggested by González *et al* (2000). The computational results predict a characteristic velocity of approximately $500 \mu\text{m}/\text{s}$, for an applied voltage of $4 V_{\text{p-p}}$. This is of two orders of magnitude higher than the experimental results. The relative shapes of the velocity profiles are similar between the experiments and computations, but with different velocity and frequency scales. This suggests that modelling AC electroosmosis as a slip boundary condition based on the tangential component of the potential gradient across the electrode surface is a valid approach. However, the method for determining the potential drop across the electric double layer, $\Delta\phi_{\text{DL}}$, may not be accurate for all conditions. It appears that the computations can be used to study, and perhaps optimise, the physical phenomena occurring in the device, but that experimental data will be required to determine the precise practical conditions under which these phenomena occur.

Acknowledgments This work has been supported by the Institute for Collaborative Biotechnologies through grant DAAD19-03-D-0004 from the U.S. Army, by AFOSR grants FA9550-04-C-0114 & FA9950-04-0106, and by NSF CTS-0404444.

References

Asbury CL, van den Engh G (1998) Trapping of DNA in non-uniform oscillating electric fields. *Biophys J* 2:1024–1030

- Bown MR, MacInnes JM, Allen RWK (2005) Micro-PIV measurement and simulation in complex microchannel geometries. *Meas Sci Technol* 16:619–626
- Chou C-F; Tegenfeldt JO, Bakajin O, Chan SS, Cox EC, Darnton N, Duke T, Austin RH (2002) Electrodeless dielectrophoresis of single- and double-stranded DNA. *Biophys J* 83(4):2170–2179
- Cummings EB, Griffiths SK, Nilson RH (2002) Ideal electrokinesis and dielectrophoresis in arrays of insulating posts. In: Applied microfluidic physics LDRD final report, Sandia National Labs, Albuquerque and Livermore
- Dai J, Ito T, Sun L, Crooks R (2003) Electrokinetic trapping and concentration enrichment of DNA in a microfluidic channel. *J Am Chem Soc* 125(43):13026–13027
- Devasenathipathy S, Santiago JG, Takehara K (2002) Particle tracking techniques for electrokinetic microchannel flows. *Anal Chem* 74:3704–3713
- Foquet M, Korfach J, Zipfel W, Webb WW, Craighead HG (2002) DNA fragment sizing by single molecule detection in submicrometer-sized closed fluidic channels. *Anal Chem* 74(6):1415–1422
- González A, Ramos A, Green NG, Castellanos A, Morgan H (2000) Fluid flow induced by nonuniform AC electric fields in electrolytes on microelectrodes. II. A linear double-layer analysis. *Phys Rev E* 61(4):4019–4028
- Green NG, Morgan H (1997) Dielectrophoretic investigations of sub-micrometre latex spheres. *J Phys D Appl Phys* 30:2626–2633
- Green NG, Morgan H, Milner JJ (1997) Manipulation and trapping of sub-micron bioparticles using dielectrophoresis. *J Biochem Biophys Methods* 35:89–102
- Green NG, Ramos A, González A, Morgan H, Castellanos A (2000) Fluid flow induced by nonuniform AC electric fields in electrolytes on microelectrodes. I. Experimental measurements. *Phys Rev E* 61:4011–4018
- Green NG, Ramos A, González A, Morgan H, Castellanos A (2002) Fluid flow induced by nonuniform AC electric fields in electrolytes on microelectrodes. III. Observation of streamlines and numerical simulation. *Phys Rev E* 66:026305
- Han J, Craighead HG (2000) Separation of long DNA molecules in a microfabricated entropic trap array. *Science* 288:1026–1029
- Ito T, Inoue A, Soto K, Hostawa K, Maeda M (2004) Single step concentration and sequence specific separation of DNA by affinity microchip. *Micro TAS* 296:159–161
- Khandurina J, Stephen C, Jacobson SC, Waters LC, Foote RS, Ramsey JM (1999) Microfabricated porous membrane structure for sample concentration and electrophoretic analysis. *Anal Chem* 71:1815–1819
- Meinhart CD, Wereley ST, Santiago JG (1999) PIV measurements of a microchannel flow. *Exp. Fluids* 27:414–419
- Meinhart CD, Wereley ST, Santiago JG (2000a) A PIV algorithm for estimating time-averaged velocity fields. *J Fluids Engng* 122:285–289
- Meinhart CD, Wereley ST, Gray MHB (2000b), Volume illumination for two-dimensional particle image velocimetry. *Meas Sci Technol* 11:809–814
- Meinhart CD, Wang D, Turner K (2003) Measurement of AC electrokinetic flows. *Biomed Microdev* 5(2):139–145
- Müller T, Gerardinov A, Schnelle T, Shirley SG, Bordoniz F, de Gasperisz G, Leonix R, Fuhry G (1996a) Trapping of micrometre and sub-micrometre particles by high-frequency electric fields and hydrodynamic forces. *J Phys D Appl Pys* 29:340–349
- Müller T, Fiedler S, Schnelle T, Ludwig K, Jung H, Fuhr G (1996b) High frequency electric fields for trapping of viruses. *Biotechnol Tech* 10(4):221–226
- Olsen MG, Adrian RJ (2000) Out-of-focus effects on particle image visibility and correlation in microscopic particle image velocimetry. *Exps Fluids (Suppl)*:S166–S174
- Przekwas A, Wang DM, Makhijani VB, Przekwas AJ (1999) Microfluidic filtration chip for DNA extraction and concentration. *IMRET* 3:488–499

- Ramos A, Morgan H, Green NG, Castellanos A (1998) AC electrokinetics: a review of forces in microelectrode structures. *J Phys D Appl Phys* 31:2338–2353
- Ramos A, Morgan H, Green NG, Castellanos A (1999) AC electric-field-induced fluid flow in microelectrodes. *J Colloid Interface Sci* 217:420–422
- Santiago JG, Wereley ST, Meinhart CD, Beebe DJ, Adrian RJ (1998) A micro particle image velocimetry system. *Exps Fluids* 25:316–319
- Tegenfeldt JO, Bakajin O, Chou C-F, Chan SS, Austin R, Fann W, Liou L, Chan E, Duke T, Cox EC (2001) Near-field scanner for moving molecules. *Phys Rev Lett* 86(7):1378–1381
- Tegenfeldt JO, Prinz C, Cao H, Huang RL, Austin RH, Chou SY, Cox EC, Sturm JC (2004) Micro- and nanofluidics for DNA analysis. *Anal Bioanal Chem* 378:1678–1692
- Tran P, Alavi B, Gruner G (2000) Charge transport along the λ -DNA double helix. *Phys Rev Lett* 85(7):1564–1567
- Van der Maarel JRC (1999) Effect of spatial inhomogeneity in dielectric permittivity on DNA double layer formation. *Biophys J* 76:2673–2678
- Wang D, Sigurdson M, Meinhart CD (2005) Experimental analysis of particle and fluid motion in AC electrokinetics. *Exps Fluids* 38(1):1–10
- Wong PK, Chen C-Y, Wang T-H, Ho C-M (2003a) An AC electroosmotic processor for biomolecules. *Transducers 2003, Boston, USA* 20–23
- Wong PK, Wang TH, Deval JH, Ho C-M (2003b) Electrokinetics in micro devices for biotechnology applications. *IEEE/ASME Trans Mechatronics* 9:366–376
- Wong PK, Chen C-Y, Wang T-H, Ho C-M (2004) Electrokinetic bioprocessor for concentrating cells and molecules. *Anal Chem* 76(23):6908–6914
- Wu J, Ben Y, Chang H-C (2005) Particle detection by electrical impedance spectroscopy with asymmetric-polarization AC electroosmotic trapping. *Microfluid Nanofluid* 1:161–167
- Zheng L, Brody JP, Burke PJ (2004) Electronic manipulation of DNA, proteins, and nanoparticles for potential circuit assembly. *Biosens Bioelectron* 20:606–619